General Disclaimer

One or more of the Following Statements may affect this Document

- This document has been reproduced from the best copy furnished by the organizational source. It is being released in the interest of making available as much information as possible.

- This document may contain data, which exceeds the sheet parameters. It was furnished in this condition by the organizational source and is the best copy available.

- This document may contain tone-on-tone or color graphs, charts and/or pictures, which have been reproduced in black and white.

- This document is paginated as submitted by the original source.

- Portions of this document are not fully legible due to the historical nature of some of the material. However, it is the best reproduction available from the original submission.

Produced by the NASA Center for Aerospace Information (CASI)

NASA

Technical Memorandum 85045

MODELING OF THE 10 MICROMETER NATURAL LASER EMISSION FROM THE MESOSPHERES OF MARS AND VENUS

D. Deming
M. Mumma

JUNE 1983

MODELLING OF THE 10-MICROMETER NATURAL LASER EMISSION

FROM THE MESOSPHERES OF MARS AND VENUS

Drake Deming and Michael J. Mumma

Infrared and Radio Astronomy Branch
NASA/Goddard Space Flight Center
Greenbelt, MD   20771

Proofs and Correspondence to:

Drake Deming
Code 693, Goddard Space Flight Center
Greenbelt, MD   20771

Suggested running head: modelling of natural laser emission

ABSTRACT

Non-thermal emission which occurs in the cores of the 9.4 and 10.4μm CO_2 bands on Mars has been recently identified as a natural atmospheric laser. The emission is believed to be excited by absorption of near-IR solar flux, followed by collisional transfer to the 00^O1 state of CO_2. A numerical model based on this mechanism is developed which includes the solar pumping contributed by $\sim2\times10^4$ near-IR CO_2 lines. The NLTE radiative transfer problem is solved to obtain the 00^O1 vibrational state population. This model successfully reproduces the existing center-to-limb observations, although higher spatial resolution observations are needed for a definitive test. The model also predicts total fluxes which are close to the observed values. The strength of the emission is predicted to be closely related to the instantaneous near-IR solar heating rate.

Calculation of the CO_2 level populations in this model supports the identification of this emission as a natural atmospheric laser. Both Mars and Venus are predicted to exhibit level inversions; at large zenith distances several percent of the emergent intensity will be due to stimulated emission. While the stimulated emission present in these lines is not large enough to be of importance to mesospheric radiative equilibrium, it has other interesting consequences. The construction of large volume radiation-pumped lasers, which utilize CO_2 planetary mesospheres as a gain medium, is theoretically possible.

I. INTRODUCTION

Strong non-thermal emission in the 9.4 and 10.4μm bands of CO_2 was first reported for the atmospheres of Mars and Venus by Betz (1976) and Betz et al. (1976), using infrared heterodyne spectroscopy. The emission occurs in the cores of the CO_2 absorption lines and is only detectable at spectral resolving powers of $\gtrsim 10^6$. The emission is believed to be formed by absorption of near-infrared solar flux, followed by collisional transfer of the absorbed quanta to the 00^01 level of CO_2, and radiative decay at 10μm. This process may be enhanced in the presence of water vapor (Johnson et al. 1976). Recently, Mumma et al. (1981) have demonstrated that in the case of Mars this emission arises from a population inversion, making it a natural laser. Theoretical pumping calculations have been given by Johnson et al. (1976), but these calculations accounted only approximately for the absorption by near-IR CO_2 bands and neglected the effect of radiative transfer in the 4.3 μm band. The understanding of this emission and its implications is still not complete, and several interesting questions remain to be answered. Although the effect of emission in these bands on the heating and cooling budgets of the Martian mesosphere is believed to be small (Ramanathan and Cess 1974), can it be a useful diagnostic tool in the study of mesospheric thermal balance in CO_2 atmospheres? To what extent is the level inversion important in this context? The emission is believed to be optically thin, however, the assumption of optical thinness may not be valid for the long atmospheric path lengths encountered by photons emitted at large zenith angles. In this case stimulated emission may have a significant effect on the emergent intensity, and could have an appreciable impact on the mesospheric cooling rate. This possibility is best considered through theoretical modelling, since current observations do not have sufficient angular resolution to impose meaningful constraints on excess limb-brightening due to stimulated emission.

This paper presents a more complete calculation of the pumping of the laser emission by including the solar pumping due to individual lines in all significant near-IR CO_2 bands. We solve the NLTE radiative transfer problem in the 4.3 μm band to obtain the population of the upper vibrational state. The possibility of significant laser amplification at large zenith distances is evaluated.

3

II. THEORETICAL CALCULATIONS

a. The atmospheric models

Prior to deriving and solving rate equations for the vibrational state populations, we must adopt model atmospheres for the mesospheres of Mars and Venus. Two essentially ad hoc model atmospheres were adopted for the Martian mesosphere (Fig. 1). The Mars models were assumed to be isothermal in the mesosphere, with temperatures bracketing the range of plausibility based on Viking measurements (Seiff and Kirk 1977). The lower temperature (120K) agrees best with our own measurements of the thermal width of the emission lines (Deming et al. 1983). The Mars models were taken to extend from the surface, at 6.3 mbars pressure, to 10^{-8} mbars, in 100 layers. The Venusian model mesosphere (Fig. 2) was taken from the Pioneer Venus "morningside model" (von Zahn et al. 1980) and day probe measurements (Seiff et al. 1980). The Venus model was assumed to extend from 10^{-8} mbars to a lower boundary at 3 mbars, in 100 layers. The models thus have an altitude resolution of ~ 0.2 scale heights. The calculated laser band emission is insensitve to the details of the model atmospheres at pressures less than $\sim 10^{-6}$ mbars, but the models were extended to higher altitudes in order to provide an adequate boundary for the 4.3μm radiative exchange calculation (described below). The laser band emission is also completely insensitive to the temperature structure of the models at pressures below ~ 0.3 mbars. Since we will be concerned with the behavior of the laser emission at extreme zenith angles, we compute optical depths using a spherical atmospheric geometry.

b. The Rate Equation for $00^{0}1$

In modelling the pumping of the laser emission we adopt the basic mechanism outlined by Betz (1976) and Johnson et al. (1976). These authors have discussed and eliminated alternative excitation processes. The mechanism for the excitation of the upper state of the laser emission, the $00^{0}1$ state, is absorption of incident solar radiation in the near-IR bands with subsequent V-V collisional transfer of the quanta to $00^{0}1$. Direct excitation of $00^{0}1$ by solar absorption at 4.3μm was neglected by Johnson et al. (1976), but we include this direct pump in our calculations. The pumping process is illustrated

4

schematically on Fig. 3. In order to calculate the source function for the
laser emission it is necessary to establish rate equations for both the $00^{0}1$
and $[(10^{0}0), (02^{0}0)]I,II$ levels. In establishing these rate equations we make
several assumptions. First, we assume that the relative populations of the
rotational levels are at their LTE values throughout the models. Since only a
few kinetic collisions are required to thermalize the rotational levels, this
assumption is valid at the pressures considered here. Second, we assume that
all ν_3 quanta, excited by absorption of solar quanta in near-IR combination
bands, are instantaneously relaxed by V-V transfer to the ν_3 fundamental state.
Third, we assume that collisional exchange of vibrational quanta from minority
isotopic forms of CO_2, to the normal isotopic form, occurs instantaneously, and
that the reverse processes never occurs. The temperature profile of the
atmosphere is regarded as fixed, and we do not couple our vibrational state
calculations to a radiative equilibrium temperature model.

Let us denote the vibrational population of $00^{0}1$ by N_2 (cm^{-3}); we similarly
denote the vibrational population of $[(10^{0}0), (02^{0}0)]_I$ by N_1. We choose to cast
the calculations for the lower levels in terms of the I level since the majority
of observations have been made in this band. For convenience, we denote
$[(10^{0}0), (02^{0}0)]_I$ as $10^{0}0$.

We can write the rate equation for N_2 as:

$$N_2 \left(A_{21} + B_{21} \int \phi_\nu^{21} J_\nu^{21} d\nu + \sum_i N_i \Omega_{21}^i \right) + \sum_{j \neq 1} N_2 \left(A_{2j} + B_{2j} \int \phi_\nu^{2j} J_\nu^{2j} d\nu \right.$$

$$\left. + \sum_i N_i \Omega_{2j}^i \right) = N_1 \left(B_{12} \int \phi_\nu^{21} J_\nu^{21} d\nu + \sum_i N_i \Omega_{12}^i \right) \quad (1)$$

$$+ \sum_{j \neq 1} N_j \left(B_{j2} \int \phi_\nu^{2j} J_\nu^{2j} d\nu + \sum_i N_i \Omega_{j2}^i + A_{j2} \right)$$

In this formulation J_ν^{ij} represents the mean intensity at frequency ν in a
band connecting vibrational states i and j; ϕ_ν^{ij} is the emission profile of the
band, and includes the individual rotational line profiles. A_{ij} and B_{ij}
represent the Einstein A and B coefficients for the vibrational transitions; in
this general notation A_{ij} is understood to be zero when state j is at higher

energy than state i. Ω^{i}_{jk} indicates the velocity-averaged collisional rate (in $cm^{+3}\ sec^{-1}$) from vibrational state j to state k, when induced by collision with a molecule in state i, i.e.:

$$CO_2(i) + CO_2(j) \xrightarrow{\quad \alpha_{jk}^{i} \quad} CO_2(k) \qquad (2)$$
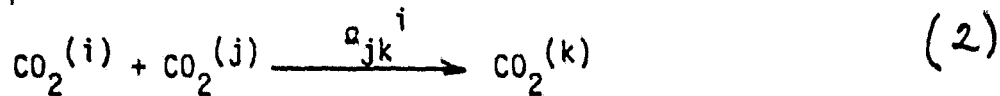
In the most general case we would also formulate similar rate equations for all other vibrational states, as well as radiative transfer equations for the bands connecting these states. Simultaneous solution of these coupled equations with the appropriate boundary conditions (e.g. solar flux incident on the top of the atmosphere) would yield all of the relevant level populations. However in the cases of interest here (primarily the mesospheres of Mars and Venus) a considerable simplification is possible. Keeping only the most significant terms from (1) we have:

$$N_2 A_{21}\ (a) + N_2 N_0 \Omega^{0}_{21}\ (b) + N_2 A_{20}\ (c)$$
$$= N_1 N_0 \Omega^{0}_{12}\ (d) + N_0 B_{02} \int \phi_{\nu}^{20} J_{\nu}^{20} d\nu\ (e) \qquad (3)$$
$$+ \sum_{j\ E_j > E_2} \nu(j) N_j N_0 \Omega^{0}_{j2}\ (f)$$

These terms represent spontaneous emission in the laser bands (a), V-T collisional de-excitation of $00^{0}1$ to $[(10^{0}0),(02^{0}0)]_{I,II}$ (b), spontaneous emission to the ground state in the 4.3 μm $00^{0}1$-$00^{0}0$ band (c), V-T collisional excitation of $00^{0}1$ from the $[(10^{0}0),(02^{0}0)]_{I,II}$ levels (d), absorption from the ground state to $00^{0}1$ (e), and V-V collisional transfer to $00^{0}1$ from higher-lying levels having one or more asymmetric stretching quanta excited (f). The factor $\nu(j)$ accounts for the fact that de-excitation of ν_3 overtones may produce more than one molecule in $00^{0}1$. We note that V-T collisional excitation and de-excitation of $00^{0}1$ has been assumed to occur through the $[(10^{0}0),(02^{0}0)]I,II$ levels. De-activation of $00^{0}1$ in laboratory studies occurs to levels with bending and symmetric stretching vibrations excited. These levels, in turn,

6

transfer vibrational quanta among themselves with large cross sections (Moore et al. 1967, Finzi and Moore 1975). The level $[(10^00),(02^00)]I,II$ is formally taken as the site of collisional transfer from 00^01, although in practice this transfer probably occurs through higher-lying levels such as $[(11^00),(03^10)]_{I,II}$.

We note that (3) contains no term representing either absorption or stimulated emission in the 10μm laser bands themselves, since these bands are expected to be optically thin. We will examine and justify this assumption later.

We can rewrite the mean intensity in (3) as:

$$J_\nu^{20} = \frac{1}{4\pi} \int_\omega I_\nu^{20}(\odot)\, d\omega + J_\nu'^{20} \qquad (4)$$

where the first term represents the solid angle average of directly incident solar photons, and $J_\nu'^{20}$ represents photons created by emission from 00^01. We can also rewrite the $N_j\Omega_{j2}^0$ terms. We write the most significant terms in the rate equation for N_j as:

$$B_{0j} N_0 \int \phi_\nu^{0j} J_\nu^{0j}\, d\nu \ (a) + N_0 N_2 \Omega_{2j}^0 \ (b)$$

$$= N_j A_{j0} \ (c) + N_0 N_j \Omega_{j2}^0 \ (d) \qquad (5)$$

This formulation accounts for direct absorption to level j (a), collisional excitation of level j from the 00^01 state (b), spontaneous emission from level j to the ground state (c) and V-V collisional de-excitation of N_j to 00^01 (d). Since the levels N_j are specified to contain one or more asymetric stretching quanta, Ω^0_{j2} will be large (Finzi and Moore 1975). We thus rewrite this rate equation as

$$N_j \, \Omega^0_{j1} \approx B_{0j} \int \phi_\nu^{0j} J_\nu^{0j} \, d\nu \qquad (6)$$

This formulation is equivalent to the assumption that all ν_3 overtone quanta excited by solar absorption are instantaneously relaxed to 00^01. The mean intensities J_ν^{0j} can be written as before:

$$J_\nu^{0j} = \frac{1}{4\pi} \int_\omega I_\nu^{0j}(0) \, d\omega + J_\nu'^{0j} \qquad (7)$$

In the case of the near-IR bands the first term, which represents the solid angle average of incident solar photons, is dominant over the self-emission of the atmosphere represented by $J_\nu^{0j'}$. We can therefore write the rate equation for 00^01 as:

$$N_2 A_{21} + N_2 N_0 \Omega^0_{21} + N_2 A_{20}$$

$$= N_1 N_0 \Omega^0_{12} + N_0 B_{02} \int \phi_\nu^{20} J_\nu'^{20} \, d\nu \qquad (8)$$

$$+ N_0 \sum_{j; \, E_j \geq E_2} \nu(j) B_{0j} \int \phi_\nu^{0j} \frac{1}{4\pi} \int I_\nu^{0j}(0) \, d\omega \, d\nu$$

where the last term now represents both direct solar excitation of 00^01 and V-V

transfer to 00^01 from ν_3 overtone levels which are excited by near-IR absorption of incident sunlight. Under conditions of interest here we may take the ground state population N_0 as equal to the total CO_2 number density. Equation (8) will be coupled to a similar equation for N_1 through the term $N_1 N_0 \Omega_{12}^0$. In practice, however, this coupling is not important and (8) can be solved for N_2/N_0 by adopting an LTE value for N_1. This is possible because at high altitudes the solar absorption term on the right side of (8) is dominant, and the $N_1 N_0 \Omega_{12}^0$ term is negligible. At lower altitudes, where the $N_1 N_0 \Omega_{12}^0$ term becomes important, collisional processes dominate in the corresponding equation for N_1. Similarly, we can include the $N_2 A_{21}$ term under the assumption that the 10μm bands are optically thin. At the lowest altitudes in the models, optical depth effects at 10μm become significant, but at these altitudes the term $N_2 N_0 \Omega_{21}^0$ dominates the left side of Eq. (8).

The principal complication in the solution of (8) occurs through the term containing $J_\nu'^{20}$. When this term is evaluated at layer i in the atmospheric model it represents the mean intensity in the 4.3μm band which is produced by emission from 00^01 in all other layers of the model. At layer i we write

$$J_\nu'^{20}(i) = \sum_j A_{20} \Delta X_j \frac{N_2(j)}{4\pi} \int_\omega \epsilon_{ji} \, d\omega \qquad (9)$$

Where ϵ_{ji} is defined as the probability that a photon emitted in the band at level j in the atmosphere will be emitted in the solid angle $d\omega$, and transmitted to level i without being absorbed in intermediate layers. ΔX_j is the geometric thickness of layer j. This integral equation formulation of the NLTE radiative transfer problem follows Dickinson (1972, 1976). Similar calculations have been performed by Kumer and James (1974). We calculate values of $\int_\omega \epsilon_{ji} d\omega$ for i,j = 1,100. This calculation is numerically tedious because each of these $100 \times 100 = 10^4$ terms involves numerical integration over ω, integration over the ∼100 rotational lines in the band and integration over ∼10^3 frequencies in each line. Moreover, Voigt profiles must be used for the rotational lines since the emission arises in the Voigt transition region of the mesosphere. We affect integration over ω by assuming azimuthal symmetry and integrating over $\mu = \cos \theta$ by 6-point gaussian quadrature, θ being defined as the angle between the zenith and the direction of photon propagation.

9

Having calculated the ϵ_{ij}, (8) reduces to a system of 100 simultaneous linear equations, which can be solved by matrix inversion or by iteration. In the present instance we have solved this system by matrix inversion. In addition to this exact solution, we also obtain an estimate for N_2 by using a "cool-to-space" approximation (Rodgers and Walshaw 1966, Dickinson 1972). This approximation removes the coupling between layers and allows us to solve each equation (8) for N_2 in terms of only local quantities. We implement this approximation in equation (8) by ignoring the term $N_0 B_{02} \int \phi_\nu^{20} \bar{J}_\nu^{20} d\nu$ and replacing $N_2 A_{20}$ with $\frac{1}{2} \langle \epsilon^{20} \rangle N_2 A_{20}$ where $\langle \epsilon^{20} \rangle$ is the angle-averaged probability that a photon emitted into the upward hemisphere escapes to the top of the atmosphere without further absorption. This "escape-to-space" probability is calculated in the same way as the $\int_\omega \epsilon_{ji} d\omega$ exchange terms. It is illustrated for the Venus model on Fig. 2. The number densities obtained for $00^{0}1$ at the pressures of relevance ($\sim 10^{-3}$ mbars) do not differ significantly when the result for the cool-to-space approximation is compared to the exact radiative exchange calculation.

In solving (8) for N_2 we adopt $A_{21} = 0.8$ sec^{-1} (Murray et al. 1974) and $A_{20} = 441$ sec^{-1} from the recent high precision measurements by Rogers et al. (198). We take $\Omega^{0}_{21} = 3.64 \times 10^{-17}T$ (cm^{+3} sec^{-1}) from Rosser et al. (1969) and Moore et al. (1967).

b. The Rate Equation for $10^{0}0$

As long as the emission is optically thin, the population of its lower state has little effect on the emergent intensity. The fact that no emission is seen in the cores of the isotopic lines argues strongly for optical thinness at disk center, but this argument cannot be used at the extreme limb because the observations have insufficient spatial resolution. Moreover, Mumma et al. claim the levels to be inverted and we wish to calculate the lower level population in sufficient detail to support or deny this claim.

The population of 10^00 is closely tied to the population of 01^10 through collisional V-V exchange. Rate equations for these two levels can be written under the cool-to-space approximation as:
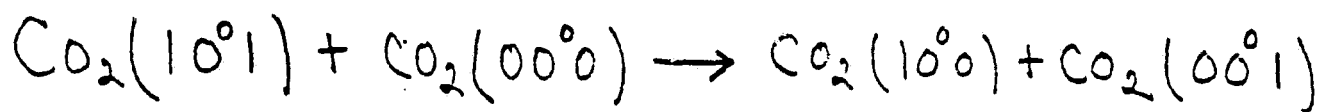
$$\sum_j \nu(j) B_{0j} \int \phi_\nu^{0j} \frac{1}{4\pi} \int I_\nu^{0j}(0)\, d\omega\, d\nu + N_0 N_2 \Omega_{21}^0 + N_2 A_{21} \quad (10)$$

$$+ N_3^2 \Omega_{31}^3 = \frac{1}{2} \langle \epsilon^{13} \rangle N_1 A_{13} + N_1 N_0 \Omega_{12}^0 + N_1 N_0 \Omega_{13}^0$$

$$N_0^2 \Omega_{03}^0 + N_0 N_1 \Omega_{13}^0 = N_3 N_0 \Omega_{30}^0 + N_3^2 \Omega_{31}^3 \quad (11)$$

$$+ \frac{1}{2} \langle \epsilon^{30} \rangle N_3 A_{30}$$

Here N_3 denotes the population (cm^{-3}) of 01^10. The first term in (10) is a solar pumping term. It occurs because solar excitation of ν_2 levels is assumed to be followed by fast (i.e. instantaneous) V-V reactions such as:

$$CO_2(10^01) + CO_2(00^00) \longrightarrow CO_2(10^00) + CO_2(00^01)$$

If V-V exchange between 10^00 and 01^10 were also instantaneous, i.e. Ω_{13}^0 and Ω_{31}^3 were very large, then solar excitation of ν_2 overtone levels could be assumed to populate 01^10 directly (e.g. Dickinson 1972). However, we used log $\Omega_{13}^0 = -13.07 + 1.368 \times 10^{-3} T$ (cm^{+3} sec^{-1}) from Bulthuis (1973). This rate, although large, is not fast enough to be considered as instantaneous, especially at the highest altitudes in our models. Other measurements, however, have given a

value of Ω^0_{13} an order of magnitude larger than the Bulthuis rate (e.g. Rhodes et al. 1968). We have therefore repeated the model calculations using an order of magnitude greater value for Ω^0_{13}. This decreases the $10^0 0$ population somewhat, leading to slightly more optical amplification in the laser bands, but has no other significant effect. In calculating the summation in Eq. (10), we assume that only solar excitation of $[(10^0 1),(02^0 1)]_{I,II}$ contributes significantly.

Since we argued that in practice N_2 can be derived independently of N_1, we can use the values of N_2 obtained from (8) in the solution of (10) and (11). We adopt $\log \Omega^0_{30} = -14.91+2.15\times10^{-3}T$ $(cm^{+3}\ sec^{-1})$ from Winter (1963). We used $A_{13}=2.9\ sec^{-1}$ from the band strength estimates of Kostkowski and Kaplan (1957) and $A_{30}=1.44\ sec^{-1}$ from Rogers et al. (1982). The angle-averaged escape-to-space functions $\langle\epsilon^{30}\rangle$ and $\langle\epsilon^{13}\rangle$ were calculated by numerical integration, as described above. An initial calculation of $\langle\epsilon^{13}\rangle$ was made by assuming an LTE population for $01^1 0$. We then solved (10) and (11) simultaneously for N_1 and N_3. Values of $\langle\epsilon^{13}\rangle$ were then recomputed using the new $01^1 0$ populations. This process was repeated until the change in the $01^1 0$ population was less than 0.1%. Since the $10^0 0$ population does not affect $01^1 0$ strongly, this iterative procedure converges rapidly.

In calculating the solar absorption terms in (8) and (10), the band profiles, $\phi^0_{\nu j}$, were represented as sums of non-overlapping rotational line profiles. The rotational lines so included were taken from the 1973 version of the AFGRL line tape (McClatchey et al., 1973). These lines were grouped by line strength and a single rotational line profile was computed as representative of each group. This profile was then replicated into the $\phi^0_{\nu j}$ profile as many times as number of lines it represented. All of the CO_2 lines on the tape were included, even isotopic lines. Many of these weaker lines give an insignificant contribution to the solar pumping. As noted earlier, excitation of ν_3 quanta by absorption in isotopic lines was assumed to transfer instantaneously to $^{12}C^{16}O_2$. The resultant profiles represent approximately 2×10^4 individual rotational lines in the region from 2000 to 9500 cm^{-1}. Using this procedure the solar flux absorbed by a group of lines could be quickly computed as proportional to the flux absorbed by the representative profile. This is a good approximation at the pressures of relevance here, because the typical line spacing is large compared to the line widths and the lines can be treated as non-overlapping. In

implementing this procedure it is necessary to recognize that this collective representation of line absorption will be temperature-dependent because of differing lower state energies for lines in a particular strength class. The distributions of line strength were accordingly recomputed for each atmospheric model, although a single distribution was used at all depths in each model. In the case of the Venus model, which is not isothermal in the mesosphere, this distribution was computed at 185K. A Voigt function was used in computing the rotational profiles, and a pressure broadening coefficient of 0.07 cm^{-1} atm^{-1} was adopted for all lines. Values of the incident solar intensity appropriate to Mars and Venus were taken from Allen (1973). The incident solar flux for Mars was based on its mean distance, the eccentricity of its orbit causes an appreciable variation ($\pm 19\%$) in this number. Calculations were made at a number of values of the solar zenith angle. The pumping line strength distributions were compiled over ~ 1500 cm^{-1} intervals, the exact value depending on the band spacings, and a single value for the incident solar intensity was used for each interval. Measured in photons cm^{-2} sec^{-1} sr^{-1} Hz^{-1} the solar intensity does not vary rapidly with frequency over the near-IR region. The most important pumping bands in each interval are listed in Table I.

Having calculated the populations of $00^{0}1$ from (8) and of $10^{0}0$ from (10) and (11), we also calculate the emergent intensity and optical depths in the core of a particular rotational line of the $00^{0}1-[(10^{0}0),(02^{0}0)]_{I}$ band, usually the 10.33μm R(8) line.

III.   RESULTS

a.   The pumping rates

Evaluation of the solar absorption terms in (8) was done separately for the four frequency intervals of interest, and the resultant pumping rates into $00^{0}1$ are shown for the 120K Mars model on Fig. 4. We confirm the claim of Johnson et al. (1976) that the 2.7μm bands, (see Table I) in the 3000-4500 cm^{-1} region, are the dominant source of pumping. However, because of the large amount of saturation at the altitude of the emission peak (~ 70 km), even the very weak lines in the 6000-9500 cm^{-1} region contribute within a factor of 3 of the 2.7μm region. We also find that, contrary to a statement by Johnson et al., direct

solar excitation of $00^{0}1$ is significant. In fact, at the highest altitudes in
the model this 2000-3000 cm^{-1} region pumping is the dominant means of exciting
$00^{0}1$.

b. The $00^{0}1$ and $10^{0}0$ level populations

The populations we calculate for the $00^{0}1$ and $10^{0}0$ levels are given on
Figs. 5 and 6 for the Mars 120K and 170K models. The corresponding calculation
for the Venus model is given on Fig. 7. In all of these models the $00^{0}1$ level
becomes inverted with respect to the $10^{0}0$ level. We therefore confirm the
claim of Mumma et al. (1981), that level inversion exists in the emitting
region. This inversion is ubiquitous at high altitudes, it appears even in
models which do not include the full set of pumping lines. In the 120K Mars
model the inversion extends down to altitudes below the emission peak; this
occurs because of the much lower thermal excitation rate for $10^{0}0$ at lower
temperature. Thus we find that the lower altitude boundary of the inverted
region depends on the kinetic temperature and on other characteristics of the
model. At high altitudes a level inversion is unavoidable in all models since
collisional excitation of $10^{0}0$ becomes unimportant, while direct solar
excitation of $00^{0}1$ is significant. Other processes, such as solar pumping of
$10^{0}0$, are not sufficient to perturb the inversion, and the ratio $N(00^{0}1)/N(10^{0}0)$
= N_2/N_1 approaches $A_{13}/A_{21} \approx 7$.

c. The height dependence of the emission

Figs. 5, 6 and 7 show the total number of photons emitted (cm^{-3} sec^{-1}) in
the 9.4 and 10.4μm bands as N_{em}. In the 170K Mars model the emission peaks at
an altitude of 75 km and drops to half intensity at 97 and 57 km. This behavior
is essentially identical to the height dependence calculated by Betz (1976) and
Johnson et al. (1976), who also used a 170K isothermal model atmosphere.
However at an altitude of ∿130 km Johnson et al. show a secondary peak in the
emission. Our preliminary models also showed this secondary peak, but it
disappears when larger numbers of pumping lines are included. The Mars 120K
model shows emission which peaks at 67 km, and falls to half intensity at 85 and
51 km. The altitude of the emission peak is thus rather insensitive to the
temperature of the model. In the case of Venus we find that the emission peaks

at 109 km and falls to half intensity at 120 and 101 km. Johnson et al. found the Venusian emission to peak at ⁓118 km, but they used a wholly different model atmosphere. This comparison again shows that the altitude for peak emission is insensitive to the details of the input model atmosphere. This is a useful result because it implies that the emission can be reliably associated with a fixed layer in the mesosphere. Repetitive observations of the frequency width of the emission cores would seem to be an excellent method for remote monitoring of temperature variability in the mesospheres of Mars and Venus.

d. Limb brightening and optical depth

Having calculated the 00^01 and 10^00 level populations, we are now in a position to calculate optical depths in the lines and to evaluate the degree of amplification which occurs because of the inversion. We have done this calculation for the core of the 10.33μm R(8) line because it is one of the strongest lines in the band, and because Deming et al. (1983) have observed it extensively. Figs. 5, 6 and 7 show the total optical depth for this line when it is observed at the sub-solar point, with the line of sight perpendicular to the solar direction. This optical depth is shown as a function of the minimum altitude along the optical path. In this computation we neglect the small variation in solar zenith distance along the line of sight and we also neglect refraction. This calculation corresponds to the case when the extreme limb of the planet is observed, and the subsolar point occurs exactly at the limb. At the extreme limb the optical depth for R(8) is negative, indicating gain in the line due to stimulated emission. In the case of the Mars 120K model the maximum gain occurs when the line of sight reaches a minimum altitude of 66 km; in this instance the optical depth is -0.07. This means that each photon which traverses the entire line of sight has a 1 in 14 chance of producing an additional photon due to stimulated emission. Since an emergent photon on average traverses only half the total distance, 4% of the emergent photons are due to stimulated emission. When the minimum altitude of the line of sight decreases to 56 km the optical depth increases to zero(!), i.e. absorption and stimulated emission exactly cancel. At this "transparent point", the region of the line of sight which lies below 60 km produces absorption, since the inversion disappears below 60 km. However this absorption is exactly cancelled by stimulated emission which occurs for those regions on the line of sight which

The relative intensity emergent from the top of the atmosphere in the core
of 10.33μm R(8) is shown as a function of angle in Fig. 8 for the 120K Mars
model. In this figure the maximum intensity emitted at large zenith angles is
more than 20 times the intensity emitted in tne zenith direction. This increase
in intensity is almost entirely due to tie increase in optical path length for
this optically thin emission; the small additional increase at the limb caused
by stimulated emission is shown by the inset to tne figure. We let θ_E be the
direction between the angle of emission and the zenith, as measured from the top
layer of the atmospheric model. We expect that emission from a very extended
plane parallel slab will peak at cos $\theta_E = 0$. The emission shown on Fig. 8 peaks
at $\cos\theta_E \sim 0.2$ because of the curvature of the atmosphere. Tne Venusian emission
is predicted to have a similar center-to-limb dependence, but it peaks at a
smaller value of cos θ_E (0.13) because the Venus atmosphere has a larger radius
of curvature.

The total relative flux (integrated over solid angle) emergent in the 9.4
and .10.4μm bands, $F_v(\theta_S)$, is shown as a function of solar zenith distance (θ_S)
for the Mars 120K model on Fig. 9. Because of the sphericity of the atmosphere
the emergent flux is not zero when the solar zenith distance is 90 degrees.
Since the emission is optically thin, we expect that the relative flux in
individual rotational lines would show the same dependence on solar zenith
distance.

Having calculated the effect of stimulated emission we can now evaluate its
importance to the physics of the atmosphere, and we can justify its omission
from the rate equation for 00^01. It is clear from Fig. 8 that stimulaied
emission will have a negligible effect on the solid angle average of the
emergent intensity and we can therefore neglect its impact on the radiative
cooling rates in the mesosphere. It is also clear that its omission from (8) is
justified because when averaged over solid angle it is insignificant in
comparison to spontaneous emission. Inclusion of a stimulated emission term in
(8) would only decrease the 00^01 population below the values we have calculated,
leading in turn to less stimulated emission. We thus conclude that laser
amplification in the 9.4μm and 10.4μm bands, while present in the mesospheres of

Mars and Venus, is of no importance in the radiative equilibrium of the atmosphere. In another context, however, the laser amplification which occurs in these lines is startlingly large, and has interesting, if somewhat speculative, consequences (see sec. g).

e. The total flux emitted

The total flux emitted by the Mars models depends on the temperature of the model. The 120K model predicts a total flux of 14.4 ergs cm^{-2} sec^{-1} and the 170K model predicts 20.6 ergs cm^{-2} sec^{-1}. The Venus model predicts a total emitted flux of 75.3 ergs cm^{-2} cm^{-2} sec^{-1}. All of these values refer to the flux emitted with the Sun at the zenith, i.e. $F_\nu(0)$. The models predict that the total emergent flux should increase as the kinetic temperature increases. At higher temperatures the radiative pumping rate into 00^01 increases. Apparently this occurs because the populations of high-J rotational levels are greater at higher temperature. Consequently many pumping lines which are weak at low temperature produce more absorption as the temperature increases. The total flux emittted in the 9.4μm and 10.4μm bands is thus predicted to be temperature sensitive through the temperature sensitivity of the pumping rate.

f. Future observations

The fluxes produced by these models are compared to observed fluxes by Deming et al. (1983). The observed Mars flux is essentially 100% of the amount predicted by the models and the Venus flux is 74% of the amount predicted. The observed fluxes are a large fraction of the model prediction. We find this somewhat surprising since a large number of pumping lines were included in the calculations, and the various approximations (e.g. non-overlapping lines) should have the net effect of overestimating the emitted flux. Presuming that our calculations are largely correct, this means that the strength of this 10μm emission is efficiently tied to the total instantaneous near-IR solar heating rate in the mesosphere. Nearly all of the bands important in near-IR heating (Dickinson 1972) are also important pumps for the 10μm emission. The strength of the 10μm emission should therefore be closely correlated with the instantaneous near-IR heating rate. Imaging of Mars and Venus, at high spatial resolution, and in a narrow frequency band containing the emission would be of

interest. If trace species such as water vapor contribute to this 10μm emission we would expect such imaging to show non-uniformities. These variations would necessarily be related to variations in the radiative heating rate, since any process which contributes to the 10μm emission will also leave CO_2 in $2\nu_2$, and this remaining energy is eventually thermalized.

g) Speculations

The laser amplification which occurs in these lines is not large by the standards of laboratory laser technology. However, the volume of gas present in the region of level inversion is vast in comparison to laboratory samples, and the total solar pumping energy deposited in this region is certainly large in comparison to the power output of laboratory lasers. This suggests that it might be possible to utilize planetary mesospheres as a natural gain medium for the construction of large-volume solar-pumped lasers. In this regard, the fact that we calculate the long-path gain in these lines to be as large as 7% is significant. This gain is sufficient to overcome reflection losses, and thus large orbiting mirrors could apparently be used to define a lasing cavity in a CO_2 planetary mesosphere. We can use the present calculations to estimate the power density that would be generated by such a cavity. In this case the rate equation (8) would be rewritten as a balance between the excitation of 00^01 through the solar pumping term, and a dominant loss term by stimulated emission. In this limit the volume emission rate becomes equal to the solar pumping rate. In the case of Venus this corresponds to $\sim 10^8$ cm^{-3} sec^{-1}. The available path length is ~ 2500 km at ~ 130 km altitude. This gives an emergent power density of $\sim 2.5 \times 10^{16}$ 10μm photons cm^{-2} sec^{-1}. This corresponds to only $\sim 5 \times 10^{-4}$ watts cm^{-2}, and so the power density obtained from such a cavity is not large. The reason for this is that the emission intensity is limited by the solar pumping rate. Yet the solar pumping occurs through absorption in the Doppler cores of the near-IR CO_2 lines. Since these Doppler cores are narrow, the pumping rate is limited by the amount of frequency space available for absorption. Formation of a cavity with orbiting mirrors would therefore not increase the volume emission rate significantly over its present value, but it would serve to impose severe directionality and bandwidth-narrowing to this emission. The power, per unit solid angle, per unit bandwidth, emergent from such a cavity could achieve extremely large values. The possibility of producing very high specific

18

intensities from such large-scale lasers may have significance for the possibility of communication with extraterrestrial intelligence (CETI). Early technical studies (e.g. Oliver 1974) concluded that such communications were best conducted in the microwave region of the spectrum. Infrared communications at 10 μm were considered, but found to be less favorable. If very high specific intensities can be obtained at 10 μm from large-scale mesospheric lasers, then these early studies should be re-assessed.

ACKNOWLEDGEMENTS

REFERENCES

Allen, C. W. (1973) Astrophysical Quantities, third edition, University of London, Athlone Press.

Betz, A. L. (1976) Ph.D. Thesis, University of California at Berkeley.

Betz, A. L., M. A. Johnson, R. A. McLaren, and E. C. Sutton (1976). Heterodyne detection of CO_2 emission lines and wind velocities in the atmosphere of Venus. Astrophys. J. 208, L141-L144.

Bulthuis, K. (1973). Laser power and vibrational energy transfer in CO_2 lasers. J. Chem. Phys. 58, 5786-5794.

Deming, D., F. Espenak, D. Jennings, T. Kostiuk, and M. Mumma (1983). Observations of the 10-Micrometer natural laser emission from the mesospheres of Mars and Venus. (accompanying paper).

Dickinson, R. E. (1972) Infrared radiative heating and cooling in the Venusian mesosphere. I. Global mean radiative equilibrium. J. Atmos. Sci. 19, 1531-1556.

Dickinson, R. E. (1976) Infrared Radiative Emission in the Venusian Mesosphere. J. Atmos. Sci. 33, 290-303.

Finzi, J. and C. B. Moore (1975). Relaxation of CO_2 (10^01), CO_2 (02^01), and $N_2O(10^01)$ vibrational levels by near reasonant V-V energy transfer. J. Chem. Phys. 63, 2285-2288.

Johnson, M. A., A. L. Betz, R. A. McLaren, E. C. Sutton and C. H. Townes (1976). Nonthermal 10-micron CO_2 emission lines in the atmospheres of Mars and Venus. Astrophys. J. 208, L145-L148.

Kostkowski, H. J. and L. D. Kaplan, (1957) Absolute intensities of the 721 and 742 cm^{-1} Bands of CO_2. J. Chem. Phys 26, 1252-1253.

Kumer, J. B. and T. C. James, (1974) CO_2 (001) and N_2 Vibrational Temperatures in the $50 \leq Z \leq 130$ km Altitude Range, J. Geophys. Res., 79, 638-648.

McClatchey, R. A., W. S. Benedict, S. A. Clough, D. E. Burch, R. F. Calfee, K. Fox, L. S. Rothman and J. S. Garing (1973). AFCRL Atmospheric Absorption Line Parameters Compilation, AFCRL-TR-73-0096.

Moore, C. B., R. E. Wood, B. Hu, and J. T. Yardley (1967). Vibrational Energy Transfer in CO_2 Lasers. J. Chem. Phys. 46, 4222-4231.

Mumma, M. J., D. Buhl, G. Chin, D. Deming, F. Espenak, T. Kostiuk and D. Zipoy (1981), Discovery of natural gain amplification in the 10μm CO_2 laser bands on Mars: a natural laser. Science 212, 45-49.

Murray, E. R., C. Kruger and M. Mitchner (1974), Measurement of 9.6-μm CO_2 laser transition probability and optical broadening cross section. Appl. Phys. Lett., 24, 180-181.

Oliver, B. M. (1974). Technical Considerations in Interstellar Communication, in Interstellar Communication: Scientific Perspectives, ed. C. Ponnamperuma and A. G. W. Cameron, Houghton Mifflin Company, Boston.

Ramanathan, V. and R. D. Cess (1974) Radiative transfer within the mesospheres of Venus and Mars. Astrophys. J. 188, 407-416.

Rhodes, C. K., M. J. Kelly and A. Javan (1968). Collisional Relaxation of the $10^0 0$ state in Pure CO_2. J. Chem. Phys. 48, 5730-5731.

Rodgers, C. D. and C. D. Walshaw (1966). The computation of infrared cooling rate in planetary atmospheres. Quant. J. Roy Meteor. Soc., 92, 67-92.

3

Rogers, J. D., Goldman, S., Rub, B. and Person, W. B. (1982). Another test of the Ability of a Fourier Transform Spectrometer to Determine Absolute Infrared Intensities. Applied Spectroscopy, in press.

Rosser, W. A., Jr., A. D. Wood and E. T. Gerry (1969). Deactivation of

Vibrationally Excited Carbon Dioxide (ν_3) by Collisions with Carbon Dioxide or with Nitrogen. J. Chem. Phys., 50, 4996-5008.

Seiff, A. and D. B. Kirk (1977). Structure of the Atmosphere of Mars in Summer at Mid-Latitudes. J. Geophys. Res. 82, 4364-4378.

Seiff, A., D. B. Kirk, R. E. Young, R. C. Blanchard, J. T. Findlay, G. M. Kelly (1980). Measurement of Thermal Structure and Thermal Contrasts in the Atmosphere of Venus and Related Dynamical Observations: Results from the Four Pioneer Venus Probes. J. Geophys. Res. 85, 7903-7933.

von Zahn, V., K. H. Fricke, D. M. Hunter, D. Krankowsky, K. Mauersberger and A. O. Nier (1980). The Upper Atmosphere of Venus During Morning Conditions. J. Geophys. Res. 85, 7829-7840.

Winter, T. G. (1963). Relaxation Time in CO_2 as a Function of H_2 and D_2 Concentration at Several Temperatures. J. Chem. Phys. 38, 2761-2765.

Figure Captions

Fig. 1   Model atmospheres adopted in the modelling of the 10μm emission from the mesosphere of Mars. The models assume an isothermal mesosphere at 120K and 170K. In situ temperature measurements by the Viking probes are shown in comparison.

Fig. 2   Model atmosphere adopted in the modelling of the 10μm emission from the mesosphere of Venus. The escape-to-space probability $\langle \epsilon^{20} \rangle$ for the 4.3μm band of $^{12}C^{16}O_2$ is also shown.

Fig. 3   Schematic of important radiative and collisional processes in CO_2, which are considered in our modelling of the 10μm laser emission. The N_i correspond to the notation used in the text for the vibrational state populations (cm^{-3}).

Fig. 4   Solar pumping rates into the ν_3 (00^01) state of CO_2 for the 120K Mars model. The pumping by different frequency regions is shown separately, labelled by frequency in cm^{-1}. The dashed line indicates the slope of the altitude dependence that would prevail for pumping by optically thin (unsaturated) absorption.

Fig. 5   Results of the model calculations for the 120K Mars model with the Sun at the zenith. The lower portion of the figure shows the calculated level populations (read left scale) for the upper (00^01) and lower (10^00) state for the 10μm emission. The dashed lines give the population of these states under the assumption of local thermodynamic equilibrium. The shaded area shows the region of level inversion. The total number of photons emitted $(cm^{-3} sec^{-1}$, read right scale), in excess of thermal emission, in the 9.4 and 10.4μm bands is shown as N_{em}. The upper half of the figure shows the total optical depth in the core of the 10.33μm R(8) line of $^{12}C^{16}O_2$. This optical depth is calculated along a line perpendicular to the local zenith and is shown ras a function of the minimum altitude along this line. The dashed porrtion of the line indicates negative optical depths, i.e. amplification in the line.

Fig. 6   Results of the model calculations for the 170K Mars model with the Sun at the zenith. See the caption of Fig. 6 for an explanation of the illustrated quantities.

Fig. 7   Results of the model calculations for the Venus model with the Sun at the zenith. See the caption of Fig. 6 for an explanation of the illustrated quantities.

Fig. 8   The modelled emergent intensity in the core of the 10.33µm R(8) line, shown as a function of angle for the 120K Mars model. The Sun is taken to be at the zenith. θ_E is defined as the angle between the zenith and the direction of propagation, as measured at the top layer of the atmospheric model. θ_p (top scale) is defined as the angle between the direction of propagation and the zenith, measured from the peak of the emission at 67 km altitude. The intensity scale is normalized to unity at $\cos\theta_E = 1.0$. The inset expands the relative intensity curve in the region of its peak. The dashed line shows the intensity obtained when laser amplification in the line is neglected.

Fig. 9   Total relative flux emitted in the 9.4 and 10.4µm laser emission shown as a function of solar zenith distance, θ_S, for the 120K Mars model. The dashed line shows a cosine dependence.

TABLE I   Principal near-infrared pumping bands. The vibrational state identifications are given as $\nu_1 \nu_2^l \nu_3^r$.

BAND ORIGIN (cm^{-1})	UPPER STATE	LOWER STATE	STRENGTH AT 120K($cm\ molecule^{-1}$)	INCIDENT SOLAR FLUX AT 1.52 AU (Photons $cm^{-2}s^{-1}/cm^{-1}$)
2336	01111	01101	1.63×10^{-19}	1.19×10^{13}
2349	00011	00001	2.36×10^{-16}	
3580	11112	01101	1.70×10^{-21}	1.62×10^{13}
3612	10012	00001	2.55×10^{-18}	
3632	10011	00001	3.95×20^{-20}	
3714	10011	00001	3.70×10^{-18}	
3723	11111	01101	2.41×10^{-21}	
4978	20012	00001	8.63×10^{-20}	2.01×10^{13}
5100	20011	00001	2.77×10^{-20}	
6972	00031	00001	3.69×10^{-21}	2.23×10^{13}

MARS MODEL ATMOSPHERES

VIKING 1
VIKING 2

ORIGINAL PAGE IS
OF POOR QUALITY
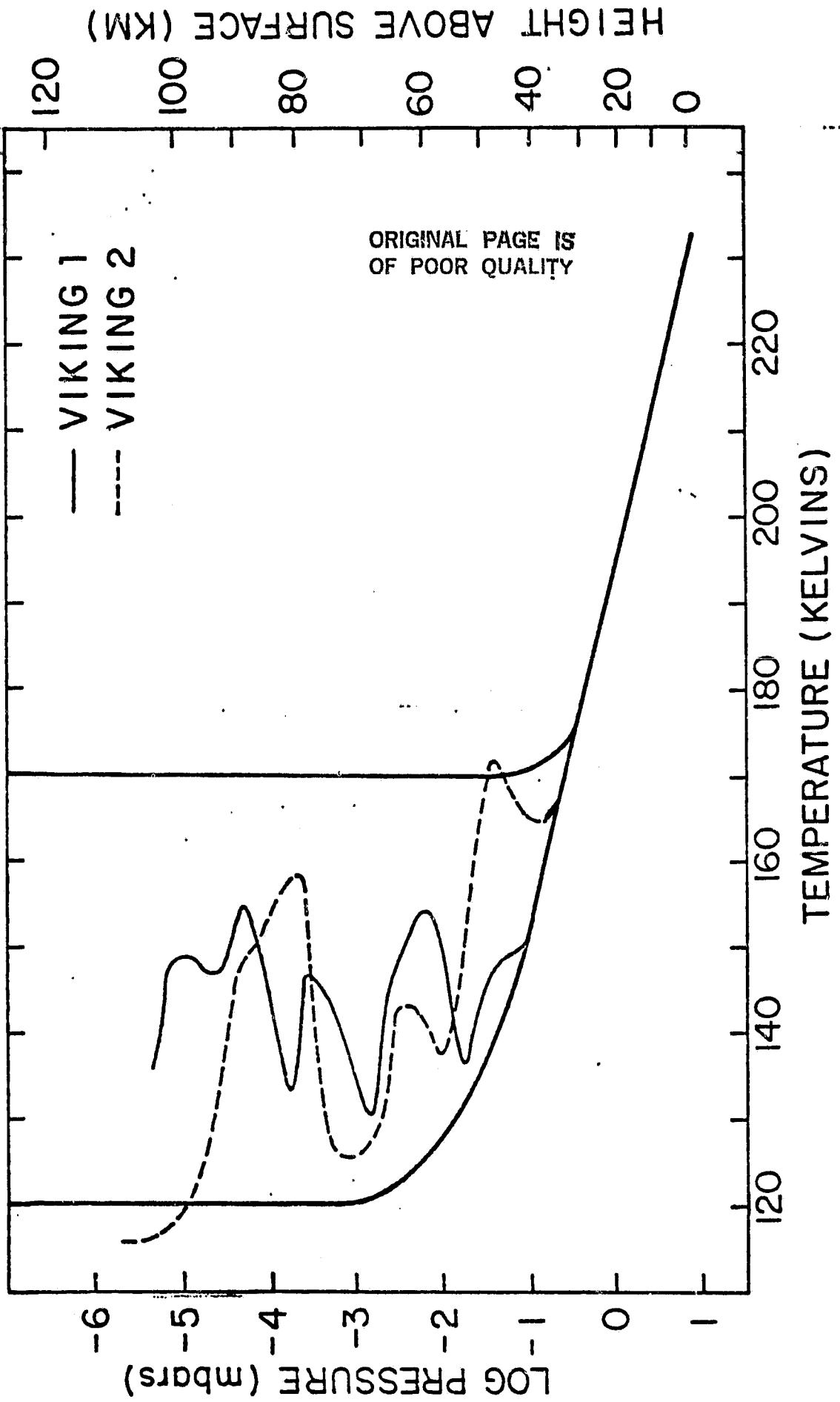
HEIGHT ABOVE SURFACE (KM)

TEMPERATURE (KELVINS)

LOG PRESSURE (mbars)

Fig. 1

Fig. 2

Fig. 3

MOLECULAR PHYSICS OF NATURAL MARTIAN LASER

Fig. 4.

Fig. 5.

Fig. 6.

Fig. 7

Fig. 8

Fig. 9.